Biomarkers Associated with Beneficial PD-1 Checkpoint Blockade in Non–Small Cell Lung Cancer (NSCLC) Identified Using High-Plex Digital Spatial Profiling

Jon Zugazagoitia[1], Swati Gupta[1], Yuting Liu[1], Kit Fuhrman[2], Scott Gettinger[3], Roy S. Herbst[3], Kurt A. Schalper[1,3], and David L. Rimm[1,3]

ABSTRACT

Purpose: Only a minority of patients with advanced non–small cell lung cancer (NSCLC) truly benefits from single-agent PD-1 checkpoint blockade, and more robust predictive biomarkers are needed.

Experimental Design: We assessed tumor samples from 67 immunotherapy-treated NSCLC cases represented in a tissue microarray, 53 of whom had pretreatment samples and received monotherapy. Using GeoMx Digital Spatial Profiling System (NanoString Technologies), we quantified 39 immune parameters simultaneously in four tissue compartments defined by fluorescence colocalization [tumor (panCK$^+$), leucocytes (CD45$^+$), macrophages (CD68$^+$), and nonimmune stroma].

Results: A total of 156 protein variables were generated per case. In the univariate unadjusted analysis, we found 18 markers associated with outcome in spatial context, five of which remained significant after multiplicity adjustment. In the multivariate analysis, high levels of CD56 and CD4 measured in the CD45 compartment were the only markers that were predictive for all clinical outcomes, including progression-free survival (PFS, HR: 0.24, $P = 0.006$; and HR: 0.31, $P = 0.011$, respectively), and overall survival (OS, HR: 0.26, $P = 0.014$; and HR: 0.23, $P = 0.007$, respectively). Then, using an orthogonal method based on multiplex immunofluorescence and cell counting (inForm), we validated that high CD56$^+$ immune cell counts in the stroma were associated with PFS and OS in the same cohort.

Conclusions: This pilot scale discovery study shows the potential of the digital spatial profiling technology in the identification of spatially informed biomarkers of response to PD-1 checkpoint blockade in NSCLC. We identified a number of relevant candidate immune predictors in spatial context that deserve validation in larger independent cohorts.

Introduction

PD-1 checkpoint blockade is standard of care and a fundamental component in the therapeutic landscape of advanced-stage non–small cell lung cancer (NSCLC). However, only a minority of patients with NSCLC truly benefits from these drugs particularly when given as monotherapies, and more robust predictive biomarkers are needed to optimally deliver these treatments (1).

Several new technologies that facilitate the assessment of multiple markers while preserving the spatial tissue architecture have been developed in recent years (2). These methodologies better characterize the tumor immune microenvironment and are promising tools for immune biomarker discovery. In fact, multiplexed IHC/immunofluorescence (IF) assays have shown to outperform the accuracy of PD-L1 expression, tumor mutational burden, and gene expression signatures for predicting response to PD-1 checkpoint blockade across several tumor types (3).

The GeoMx Digital Spatial Profiling (DSP) System (NanoString Technologies) is a new platform that enables simultaneous antibody-based detection of multiple proteins from single formalin-fixed, paraffin-embedded (FFPE) tissue sections in a quantitative and spatially resolved manner (4). Because of its high-fold multiplexing capacity from specific regions or marker-selected tissue compartments of interest, it is well suited for the identification of novel spatially informed tissue biomarkers. In this study, we used DSP technology as a discovery tool to find spatially resolved protein markers associated with benefit from single-agent PD-1 checkpoint blockade in advanced NSCLC. Then, among the identified candidate predictors, we further assessed CD56 expression by multiplex IF and cell count quantification, with the aim to prove reproducibility in terms of outcome association with an orthogonal quantitative method.

Materials and Methods

Patient cohort and tissue microarrays

We analyzed retrospectively collected FFPE tumor specimens represented in a tissue microarray (TMA) format from 81 patients with NSCLC treated with PD-1 checkpoint blockade in the advanced setting between 2009 and 2017 at Yale University School of Medicine (New Haven, CT; YTMA404). All tissue samples were collected and used under the approval from the Yale Human Investigation Committee protocol #9505008219 with an assurance filed with and approved by the U.S. Department of Health and Human Services. The Yale Human Investigation Committee approved the patient

[1]Department of Pathology, Yale University School of Medicine, New Haven, Connecticut. [2]NanoString Technologies, Seattle, Washington. [3]Department of Medicine (Oncology), Yale University School of Medicine and Yale Cancer Center, New Haven, Connecticut.

Note: Supplementary data for this article are available at Clinical Cancer Research Online (http://clincancerres.aacrjournals.org/).

Current address for J. Zugazagoitia: Department of Medical Oncology, Hospital Universitario 12 de Octubre, Madrid, Spain; and current address for Swati Gupta, H3 Biomedicine, Cambridge, Massachusetts.

Corresponding Author: Jon Zugazagoitia, Hospital 12 de Octubre, Madrid 28040, Spain. Phone: 349-1390-8003; Fax: 249-1390-8349; E-mail: jonzuga@gmail.com

Clin Cancer Res 2020;26:4360–8

doi: 10.1158/1078-0432.CCR-20-0175

Translational Relevance

The majority of patients with advanced non–small cell lung cancer (NSCLC) do not respond to PD-1 axis blockade, and more robust predictive biomarkers are needed. Using the digital spatial profiling (DSP) system, we identified 12 protein markers independently associated with benefit from single-agent PD-1 checkpoint blockade in spatial context. High expression of CD56 and CD4 in the CD45 compartment were significantly associated with all favorable clinical outcomes, whereas high levels of VISTA and CD127 in the tumor compartment were markers associated with immunotherapy resistance. We also validated the DSP finding that high $CD56^+$ immune cell counts in the stroma were predictive for progression-free survival (PFS) and overall survival (OS) in the same set of patients using multiplex immunofluorescence, strengthening the relevance of natural killer (NK)/NK T cells as a candidate predictive biomarker for immunotherapy in NSCLC. This work identifies a number of relevant candidate predictors of immunotherapy outcome in spatial context that show promise for future validation in larger independent cohorts.

informed consent or in some cases waiver of consent all in accordance with the ethical guidelines of the U.S. Common Rule.

For TMA construction, tumors were reviewed by a local pathologist using hematoxylin and eosin–stained preparations to select representative tumor areas. Then, two cores (0.28 mm^2 each) were extracted from each tumor block and arrayed in two recipient TMA master blocks, each TMA block thus containing one nonadjacent 0.28 mm^2 tumor core per NSCLC case. Tumor core selection was not based on specific tumor segments or location.

For all the experiments, we assessed two slides derived from two independent YTMA404 blocks, each block containing one nonadjacent tumor core per patient. A total of 67 cases included in YTMA404 had available or adequate histospots for protein quantification. Of these, 53 had preimmunotherapy specimens and received single-agent PD-1 checkpoint blockade, constituting our discovery cohort (see consort diagram, Supplementary Fig. S1). **Table 1** summarizes the clinicopathologic characteristics of these patients.

DSP

Briefly, once the slides were deparaffined and subjected to antigen retrieval procedures, we coincubated them overnight with three fluorescent-labeled visualization antibodies to detect tumor cells [pan-cytokeratin (CK)], all immune cells (CD45), and macrophages (CD68), together with a cocktail of 44 unique photocleavable oligonucleotide-labeled primary antibodies targeting immuno-oncology markers (Supplementary Table S1). Once the staining was completed, we loaded the slides in a prototype Beta version of the GeoMx DSP instrument, where they were scanned to produce a digital fluorescent image of the tissue. Next, we generated individual regions of interest (ROI) of a maximum of 0.28 mm^2 covering the entire TMA core, then each ROI was segmented in four molecularly defined tissue compartments by fluorescent colocalization: tumor compartment ($panCK^+$), immune cell compartment ($CD45^+$), macrophage compartment ($CD68^+$), and nonimmune cell stroma compartment ($SYTO13^+$/$panCK^-$/$CD45^-$/$CD68^-$; **Fig. 1**). Oligos from these compartments were released upon exposure to UV light in a sequential manner to the macrophage, immune cell, tumor, and finally nonimmune cell stromal compartments. Photocleaved oligos were collected via microcapillary

Table 1. Clinical-pathologic characteristics of the discovery cohort.

Characteristic	Number of patients (%)
Total patients with evaluable tumors	53
Treatment	
Nivolumab	45 (86)
Pembrolizumab	6 (6)
Atezolizumab	4 (8)
Gender	
Female	24 (45)
Male	29 (55)
Age	
<70 years	23 (44)
≥70 years	30 (57)
Performance status	
0–1	46 (87)
>1	7 (13)
Smoking	
Ever smoker	46 (87)
Never smoker	7 (13)
Histology	
Adenocarcinoma	38 (72)
Squamous-cell carcinoma	12 (23)
Large-cell carcinoma	3 (5)
Type and site of tumor specimen	
Lung primary	37 (70)
Non–lymph node metastasis	7 (13)
Lymph node metastasis	9 (17)
Stage	
III	1 (2)
M1a	13 (24)
M1b	9 (17)
M1c	29 (55)
Liver metastasis	
Yes	11 (21)
No	41 (77)
Missing	1
Mutation status	
EGFR	5 (9)
KRAS	15 (28)
Others	5 (9)
Wild-type	28 (53)
Derived neutrophil to lymphocyte ratio	
≤3	35 (66)
>3	16 (30)
Missing	2
LIPI score	
Good	22 (41)
Intermediate	19 (36)
Poor	3 (6)
Missing	9
Prior systemic therapies for advanced disease	
0	9 (17)
1	27 (51)
>1	17 (32)
Best response to immunotherapy	
Partial response	6 (11)
Stable disease	18 (34)
Progressive disease	27 (51)
Not evaluable	2
Benefit from immunotherapy[a]	
CB	16 (30)
NCB	35 (66)
Not evaluable	2

Abbreviations: CB, clinical benefit; NCB, nonclinical benefit.
[a]We defined CB as having experienced partial response or stable disease lasting ≥6 months as best response, whereas NCB was defined as primary progressive disease or stable disease lasting <6 months.

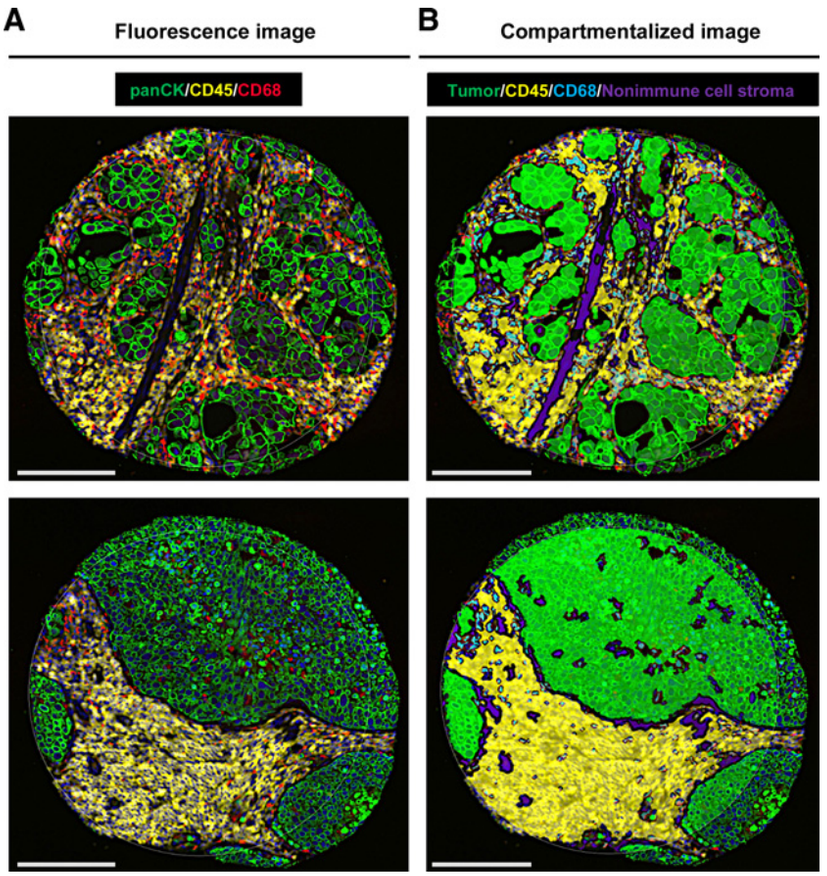

Figure 1.
Representative TMA spots showing the fluorescence image (**A**) and the compartmentalized image created by fluorescence colocalization (**B**) using GeoMx DSP (scale bar, 100 μm).

aspiration and dispensed into a 96-well plate, then hybridized to 4-color, 6-spot optical barcodes and finally digitally counted in the nCounter System (NanoString Technologies). Digital counts from barcodes corresponding to protein probes were first normalized to internal spike-in controls (ERCC), and then normalized to the area of their compartment. We systematically excluded those compartments with less than 10 nuclei or an area of illumination (AOI) less than 100 μm^2. A more detailed description of the protocol can be found in Supplementary Materials and Methods.

Multiplexed IF natural killer-cell panel and cell counting

We performed a multiplexed IF staining protocol for simultaneous detection of CK^+ tumor cells, $CD3^+$ lymphocytes, and $CD56^+$ cells. The protocol is detailed in Supplementary Materials and Methods.

We determined cell counts using the inForm Tissue Finder Software (Akoya) on multispectral images acquired using a Vectra 3 System (PerkinElmer), as described previously (ref. 5; Supplementary Materials and Methods). First, automated tissue segmentation identified tumor and stroma regions, and two tissue compartments were generated: tumor compartment ($DAPI^+/CK^+$) and nontumor or stromal compartment ($DAPI^+/CK^-$). Therefore, in this case, the stromal compartment includes both the $CD45^+$ immune cell compartment and the nonimmune cell stromal compartment that were separately generated with DSP. Next, cell segmentation within these regions identified individual cells and respective nuclei, cytoplasm, and membrane components using signal in the nucleus and membrane as internal and external cell borders. Cells were phenotyped on the basis of fluorescent marker intensity then we calculated the number of individual cell populations as a percentage of the total number of cells in the tumor compartment, the stromal compartment, and the entire TMA core.

Statistical analysis

Pearson correlation coefficient was used to analyze the agreement between target counts derived from different tumor regions. For further statistical analysis, we averaged the normalized digital counts or cell counts derived from the two YTMA404 blocks. We stratified each NSCLC case into high and low expression using two exploratory cut-off points, median and top tertile. We analyzed the association between target expression and clinical benefit (CB; **Table 1**; Supplementary Materials and Methods) using binary logistic regression models or the nonparametric Mann–Whitney test. Survival curves were computed with the Kaplan–Meier product-limit method and compared using the log-rank test. We calculated HRs for progression-free survival (PFS) and overall survival (OS) using the Cox proportional hazard model. To provide more stringent control on false-positive results, we used the Benjamini–Hochberg false discovery adjustment method. We applied multiplicity adjustments for PFS and OS associations considering the number of comparisons performed per compartment (tumor, CD45, and CD68), and separately for median and top tertile cut-off point comparisons. All hypothesis testing was performed at a two-sided significance level of $\alpha = 0.05$.

Table 2. Markers significantly associated with PFS and/or OS benefit under PD-1 checkpoint blockade.

Markers associated with PFS benefit									
Compartment	**Marker**	**Cut-off point**	**Log-rank *P***	**Adjusted log-rank *P***	**Univariate HR (95% CI)**	***P***	**$P_{adjusted}$**	**Multivariate HR (95% CI)**	***P***
Tumor compartment	**VISTA**	Top tertile	0.001	**0.014**	2.60 (1.37–4.92)	0.003	**0.043**	2.49 (1.15–5.40)	**0.020**
	CD127	Top tertile	0.001	**0.014**	2.65 (1.41–4.98)	0.002	**0.043**	2.39 (1.07–5.34)	**0.033**
CD45 compartment	CD56	Top tertile	0.004	0.124	0.38 (0.18–0.80)	0.011	0.341	0.24 (0.08–0.66)	**0.006**
	CD4	Median	<0.001	<**0.001**	0.33 (0.16–0.67)	0.002	0.062	0.31 (0.12–0.76)	**0.011**
	ARG1	Median	0.006	0.18	0.43 (0.21–0.86)	0.018	0.279	0.37 (0.16–0.83)	**0.016**
CD68 compartment	CTLA4	Top tertile	0.023	0.736	1.95 (1.01–3.77)	0.044	0.858	2.36 (1.06–5.25)	**0.035**

Markers associated with OS benefit									
Compartment	**Marker**	**Cut-off point**	**Log-rank *P***	**Adjusted log-rank *P***	**Univariate HR (95% CI)**	***P***	**$P_{adjusted}$**	**Multivariate HR (95% CI)**	***P***
Tumor compartment	STING	Top tertile	0.002	0.058	0.31 (0.14–0.69)	0.004	0.116	0.33 (0.12–0.89)	**0.029**
CD45 compartment	CD45	Median	0.003	**0.022**	0.35 (0.16–0.73)	0.005	**0.045**	0.47 (0.15–1.44)	0.19
	CD56	Top tertile	0.033	0.127	0.44 (0.20–0.97)	0.044	0.169	0.26 (0.09–0.75)	**0.014**
	PD-L1	Median	0.038	0.167	0.48 (0.23–0.99)	0.049	0.20	0.43 (0.15–1.23)	0.11
	CD68	Top tertile	0.024	0.119	0.43 (0.20–0.93)	0.033	0.159	0.16 (0.05–0.47)	**0.001**
	CD4	Median	0.001	**0.015**	0.31 (0.15–0.66)	0.002	**0.030**	0.23 (0.08–0.66)	**0.007**
	B2M	Median	0.001	**0.015**	0.28 (0.12–0.61)	0.002	**0.030**	0.35 (0.12–0.96)	**0.041**
	CD20	Median	0.008	0.048	0.38 (0.18–0.82)	0.014	0.084	0.83 (0.32–2.16)	0.71
	CD3	Median	<0.001	<**0.001**	0.24 (0.11–0.53)	<0.001	<**0.001**	0.24 (0.09–0.64)	**0.005**
	CD8	Top tertile	0.016	0.117	0.38 (0.17–0.87)	0.023	0.159	0.54 (0.21–1.39)	0.20
	TIM3	Median	0.003	**0.022**	0.32 (0.14–0.72)	0.006	**0.045**	0.62 (0.24–1.60)	0.32
	CD40	Median	0.039	0.167	0.48 (0.24–0.99)	0.049	0.20	0.47 (0.17–1.28)	0.14
	ICOS	Top tertile	0.006	0.093	0.35 (0.16–0.78)	0.010	0.155	0.26 (0.08–0.79)	**0.018**
CD68 compartment	CD45	Top tertile	0.004	0.064	0.33 (0.15–0.74)	0.008	0.128	0.31 (0.11–0.87)	**0.026**
	PD-L1	Top tertile	0.035	0.243	0.45 (0.21–0.98)	0.045	0.288	0.55 (0.22–1.39)	0.17
	CD20	Top tertile	0.004	0.064	0.33 (0.14–0.74)	0.007	0.128	0.56 (0.21–1.45)	0.23
	GNZB	Top tertile	0.023	0.243	0.42 (0.18–0.93)	0.032	0.288	0.55 (0.20–1.47)	0.23

Note: Bold terms are *P* values that are significant after adjusting for multiple comparisons and/or after controlling for clinical prognostic factors in the multivariate analysis.

Results

We generated 135 ROIs from 67 NSCLC cases, each represented by two TMA cores in two YTMA404 master blocks. Each ROI was compartmentalized in four tissue compartments, from which 39 protein markers (excluding controls) were separately measured, resulting in 156 quantitative variables per ROI.

First, to assess the performance of the assay, we evaluated the normalized counts of each target relative to nonspecific counts (background). To estimate background levels, we averaged the counts from three negative isotype controls for each NSCLC case (Supplementary Table S1). Most targets showed high signal relative to nonspecific counts across all samples (Supplementary Fig. S2). Five markers (PD-1, LAG3, GITR, CD86, and CD40L) showed low signal to background ratios (<3) across all four tissue compartments in more than 95% of the TMA spots, and were considered not evaluable for outcome analysis (Supplementary Figs. S1 and S3).

To internally validate the reproducibility of DSP, and also to test the concordance of target count measurements between nonadjacent tumor areas, we compared target counts from each of the two independent cores from each patient, collected in separate DSP runs. In general, abundantly expressed markers in the tumor compartment (e.g., STING or HLA-DR) showed high R^2 values ($R^2 > 0.6$), whereas less abundant or heterogeneous markers (e.g., CD3 in the tumor compartment or PD-L1 in the CD45 compartment) showed lower R^2 values (Supplementary Fig. S4).

Then, we evaluated the association between spatially informed marker expression and outcome in 53 patients treated with single-agent PD-1 checkpoint blockade. For this analysis, we only included those NSCLC cases with sufficient compartment area for accurate target measurement (≥10 nuclei or ≥100-μm^2 AOI) in the tumor compartment ($n = 52$), CD68 compartment ($n = 47$), and CD45 compartment ($n = 42$; Supplementary Figs. S1 and S5). Target counts from nonimmune cell stroma were considered inadequate for outcome assessment, because immune markers in this compartment were expressed at very low levels (Supplementary Fig. S6).

In the univariate unadjusted analysis using two exploratory cut-off points, we found 18 markers associated with PFS and/or OS in spatial context (**Table 2**). After multiplicity adjustment, five markers remained significantly associated with outcome: VISTA and CD127 in the tumor compartment, and CD4, Beta-2 microglobulin, and CD3 in the CD45 compartment (**Table 2**). In the multivariate analysis including four clinical prognostic factors [performance status, smoking history, presence of liver metastasis, and lung immune prognostic index (LIPI) score], high levels of CD56 (top tertile) and CD4 (median) measured in the CD45 compartment were the only markers that were predictive for all clinical outcomes, including durable CB (Supplementary Table S2), longer PFS (HR: 0.24, $P = 0.006$; and HR: 0.31, $P = 0.011$, respectively), and prolonged OS (HR: 0.26, $P = 0.014$; and HR: 0.23, $P = 0.007$, respectively; **Table 2** and **Fig. 2**). In contrast, high levels of VISTA (top tertile) and CD127 (top tertile) in the tumor compartment significantly predicted nonclinical benefit (NCB; Supplementary Table S2) and shorter PFS (HR: 2.49, $P = 0.020$; and HR: 2.39, $P = 0.033$, respectively),

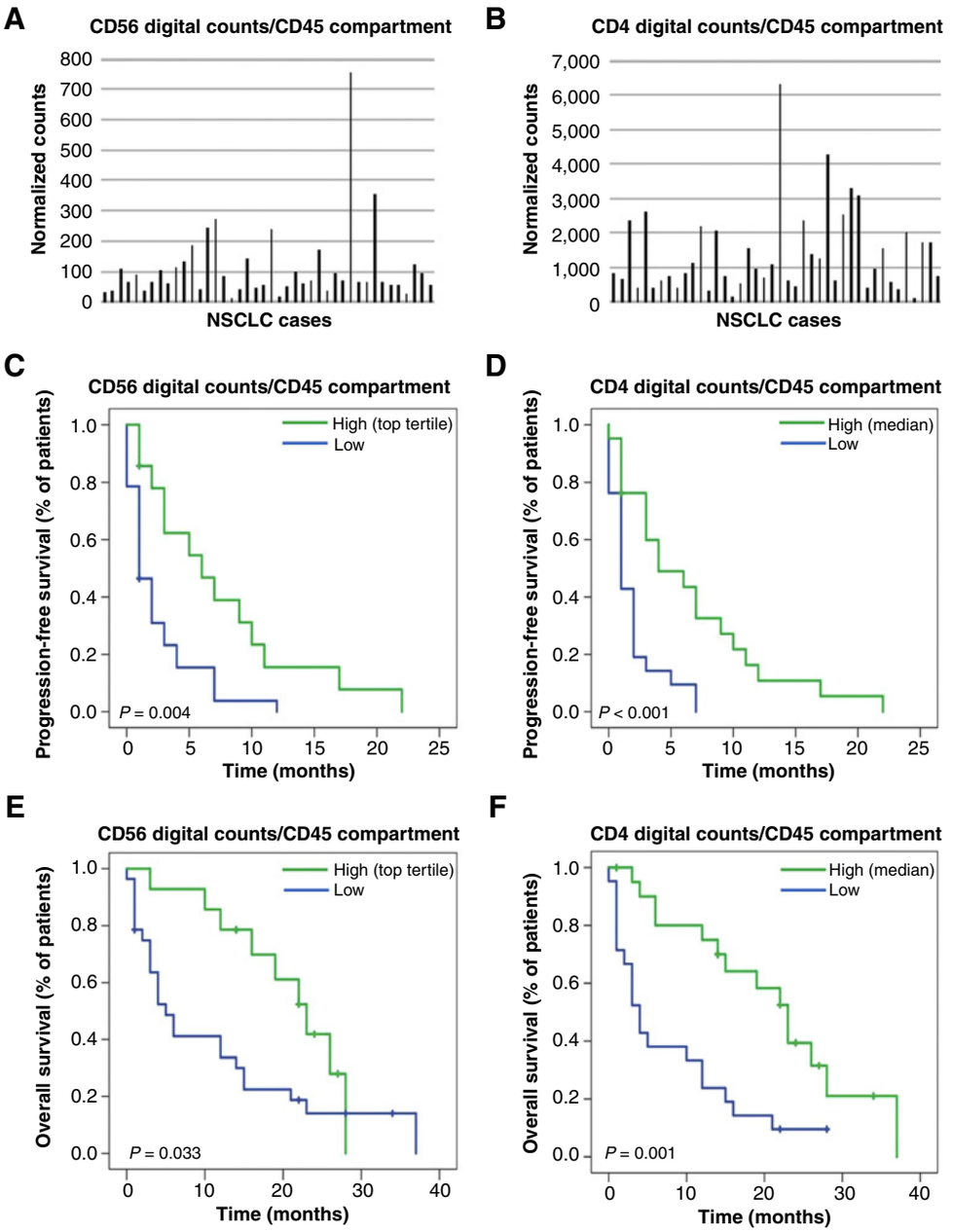

Figure 2.

CD56 and CD4 expression in the CD45 compartment measured by digital counts and their association with outcome. **A** and **B,** Histogram showing the distribution of CD56 digital counts (**A**) and CD4 digital counts (**B**) in YTMA404 ($n = 42$). PFS according to CD56 digital counts in the CD45 compartment (top tertile; **C**) and CD4 digital counts in the CD45 compartment (median; $n = 42$; **D**). OS according to CD56 digital counts in the CD45 compartment (top tertile; **E**) and CD4 digital counts in the CD45 compartment (median; $n = 42$; **F**).

although OS differences did not reach statistical significance (**Table 2**). In this cohort, high PD-L1 expression in the CD45 compartment and the CD68 compartment was associated with longer OS in the univariate analysis (log-rank $P = 0.038$ and $P = 0.035$, respectively), although it did not hold significance after adjusting for multiple testing or for clinical prognostic factors in the multivariate model. High PD-L1 expression in the tumor compartment did not show any significant association with outcome (**Table 2**).

Finally, to be certain that high levels of CD56 in immune cell stroma were associated with longer PFS and OS in our cohort, we determined its expression using an orthogonal fluorescent-based cell count method in serial YTMA404 sections. For that purpose, we developed a multiplex IF panel to discriminate between $CD56^+$ tumor cells ($CD56^+/CK^+$) and $CD56^+$ immune cells [$CD56^+/CK^-$, which included $CD56^+/CD3^-$ natural killer (NK) cells and $CD56^+/CD3^+$ NK T (NKT) cells]. Representative images of these cell phenotypes

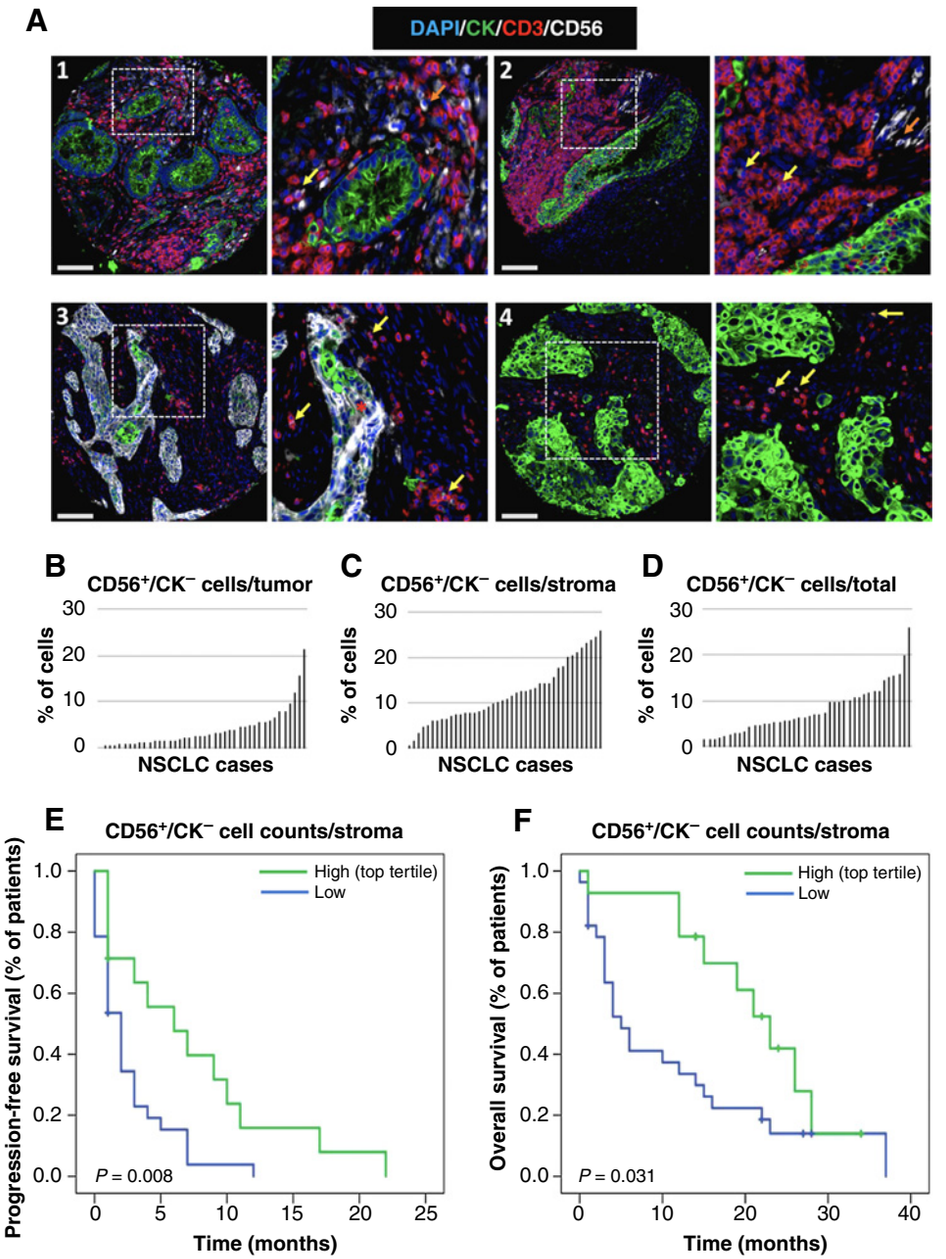

Figure 3.

Orthogonal validation of $CD56^+/CK^-$ cell counts assessed by inForm as predictors of outcome in YTMA404 cohort. **A,** Representative images acquired with Vectra Polaris microscope showing CD56 staining pattern in four NSCLC cases (scale bar, 100 μm). CK^+ tumor cells are shown in green, $CD3^+$ T cells in red, and $CD56^+$ cells in white. Orange arrows indicate $CD56^+$ NK cells and yellow arrows indicate $CD3^+/CD56^+$ NKT cells. Panel 3 illustrates an NSCLC case with strong CD56 positivity in the tumor compartment, and the red asterisk highlights $CD56^+/CK^+$ tumor cells. Distribution of $CD56^+/CK^-$ cells in the tumor compartment (**B**), the stromal compartment (**C**), and entire TMA spot (**D**; $n = 42$). PFS (**E**) and OS (**F**) according to $CD56^+/CK^-$ cell counts (top tertile) in YTMA404 cohort ($n = 42$).

acquired with the Vectra system are shown in **Fig. 3**. The median percentage of $CD56^+/CK^-$ cells from total cells across NSCLC cases were 7%, and were primarily found in the stromal compartment (**Fig. 3B–D**). The distribution of absolute $CD56^+/CK^-$ cell counts per compartment can be found in Supplementary Fig. S7A–S7C. Using the top tertile cut-off point in the same 42 NSCLC cases, we found that $CD56^+/CK^-$ cell counts in the stromal compartment were also associated with longer PFS and OS (**Fig. 3E** and **F**). Patients with CB had a significantly higher median percentage of $CD56^+/CK^-$ cells in the stroma (20.5%) as compared with those with NCB (9.7%; $P = 0.027$). When analyzed as absolute cell counts, patients with CB also had a higher median number of stromal $CD56^+/CK^-$ cells (85 cells vs. 28 cells), but this difference did not reach statistical significance ($P = 0.49$; Supplementary Fig. S7D and S7E). We further explored the predictive significance of $CD56^+/CD3^-$ NK cells and $CD56^+/CD3^+$ NKT cells independently. We observed a stronger trend toward an association with PFS and OS for $CD56^+/CD3^+$ cells as compared with $CD56^+/CD3^-$ cells, but neither of them were significantly associated with outcome when measured separately (Supplementary Fig. S8).

Discussion

In this pilot scale discovery study, we show the potential of the DSP technology in the identification of spatially informed biomarkers of CB to PD-1 checkpoint blockade in NSCLC. By combining high-fold

multiplexing with spatial resolution, we identified 12 markers that were associated with PFS and/or OS benefit in spatial context, independently from clinical prognostic factors.

Perhaps one of the most relevant finding in this study is the identification of high levels of CD56 and CD4 in the CD45 compartment as predictors of all favorable clinical outcomes, including CB, longer PFS, and prolonged OS. Although CD56 expression did not hold significant after adjusting for multiple testing, it was significant in the multivariate analysis, and its association with outcome was further validated with an orthogonal method. In this cohort, CD8 levels in the CD45 compartment only predicted longer OS in the univariate analysis, with no differences in terms of CB or PFS. Collectively, these findings support the notion that antitumor immune responses following PD-1 checkpoint blockade are likely not exclusively mediated by cytotoxic CD8 T cells, and that NK cells and CD4 T cells also play a role in therapeutic efficacy (6–8).

Our results related to NK cells are concordant with several studies conducted in melanoma cohorts that have shown that NK-cell gene signatures correlate with responsiveness from immunotherapy (9, 10). In another study, circulating $CD56^+$ cells detected by mass cytometry (CyTOFF) were shown to be upregulated in patients with melanoma that responded to PD-1 checkpoint blockade (11). We now extend these findings to NSCLC, having identified an association between CD56 expression in the immune cell stroma and better treatment outcome. By using a multiplex IF panel targeting CD56 and CD3, we quantitatively assessed the abundance of $CD56^+$ NK cells and NKT cells within the tumor microenvironment. Using inForm, we confirmed that these cells were mostly localized in the stroma. Notably, we could reproduce the outcome association by inForm cell count quantification method, with a degree of benefit that compared very similarly with the outcome association obtained when measuring CD56 expression in the $CD45^+$ immune cell compartment (part of the stromal compartment in inForm analysis) using DSP. These results suggest that NK/NKT cells are likely localized mostly in the $CD45^+$ compartment within the stroma, although the absence of CD45 compartmentalization with inForm precludes us to draw definitive conclusions in this regard. We believe that this orthogonal validation, although performed in the same set of patients, strengthens the value of $CD56^+$ immune cells as a candidate predictor of outcome from PD-1 checkpoint blockade in NSCLC.

In-line with the findings in our study, it has been suggested that CD4 T cells might play an equally relevant or perhaps more central role than CD8 T cells in mediating efficacy from anticancer immunotherapy (6, 12). In a prospective study conducted in patients with NSCLC, functional systemic CD4 immunity was required for deriving significant benefit from PD-1 checkpoint blockade (13). Also, CD4 counts measured in a CD45-defined compartment using DSP was one of the immune parameters associated with longer disease-free survival in patients with melanoma treated with neoadjuvant immune checkpoint blockade (14).

The identification of high levels of VISTA and CD127 expression in the tumor compartment as predictors of immunotherapy resistance is also a remarkable finding. Upregulation of compensatory inhibitory checkpoints (including VISTA) has been previously reported as an acquired resistance mechanism to PD-1 checkpoint blockade (15, 16). To our knowledge, the role of CD127 (IL7R) signaling in mediating immunotherapy response in solid tumors has not been described previously. A study conducted in curatively resected NSCLC also found that tumor cell expression of IL7R was associated with shorter disease-free survival and OS (17), highlighting a potential poor prognostic role of IL7R signaling in NSCLC.

This study found that PD-L1 expression in immune cells but not tumor cells was associated with OS in the univariate analysis. This reproduces our previous finding with quantitative IF in the same cohort (18). Furthermore, it is also consistent with another study by our group performing DSP in melanoma, where macrophage PD-L1 carried the sensitivity to predict immunotherapy outcomes (19). These findings are in-line with previous studies that have shown that targeting PD-1/PD-L1 axis can still be effective regardless of PD-L1 tumor expression (20). Mechanistic studies in mouse models also support macrophages expressing PD-L1 as the key effector cells mediating tumor regression following PD-1 axis blockade (21, 22). However, in our study, PD-L1 expression by immune cells and macrophages did not reach significance after controlling for clinical factors or adjusting for multiple testing.

Regarding the potential clinical applicability of the findings in this study, first we need to consider that the recent approval and increasing use of chemoimmunotherapy combinations in the first-line setting has limited the use of single-agent PD-1 axis blockade in unselected NSCLC patients. Monotherapy with PD-1 axis inhibitors is now mostly restricted to patients with high PD-L1 expression, where the response rate is substantially higher (about 45%; ref. 1) as compared with the response rate observed in our unselected cohort. Therefore, future biomarker discovery studies will preferably need to focus on subgroups of patients with NSCLC with high PD-L1 [tumor proportion score (TPS) $\geq$ 50%] treated with monotherapy, and unselected patients treated with chemoimmunotherapy combinations. If the findings from this study are confirmed in these cohorts, this could suggest that future companion diagnostic tests to predict immunotherapy outcomes may require measuring markers from particular tissue compartments or colocalized with specific cell types (e.g., $CD45^+$ cells). The DSP system is well suited for this aim, utilizing FFPE tumor samples with a relatively simple workflow. Therefore, although still many future efforts are needed to demonstrate the utility of the DSP system to inform therapeutic decisions and impact clinical care, with the appropriate validation it could be potentially scalable as a clinical assay in a Clinical Laboratory Improvement Amendments laboratory in the future.

This study has to be interpreted in the context of a number of limitations. First, it is underpowered to demonstrate the independent predictive value for PD-L1 expression. Our cohort is a retrospective collection of tumors from patients treated in routine practice at a single institution, not a clinical trial. Furthermore, this is a single cohort study in which we assessed multiple hypotheses. Although we applied statistical correction for multiple testing, the false discovery adjustment method that we used is conservative, and does not preclude the need for validation in independent cohorts. As such, the data presented here must be considered hypothesis generating data, and require validation in future external cohorts. It is also a limitation that we used a TMA instead of whole-tissue sections. Although we assessed two nonadjacent tumor cores, we recognize that this still represents a small percentage of the area of the standard tissue section. This could potentially under or overrepresent biomarker expression due to the heterogeneity of the tumor immune microenvironment and potentially influence biomarker performance, particularly for those heterogeneous immune parameters that are expressed at relatively lower levels. Therefore, future validation efforts should include whole-tissue sections assessing a greater number of ROIs. In this same line, the vast majority of the tumor samples included in the TMA and assessed in this study were primary tumors or lymph node biopsies, and mostly from patients that received PD-1 axis inhibition as second or further line of treatment. We tried to perform subgroup analysis and bivariate

Cox proportional hazards models to explore whether the outcome association differed depending on biopsy site (primary/locoregional vs. distant metastasis) or line of therapy (first-line vs. later line), but the subgroups were too small to draw meaningful conclusions in this regard (Supplementary Tables S3 and S4). Finally, another limitation is perhaps inherent to the DSP protein detection assay. Five markers included in the panel had poor signal to background ratios in nearly all samples, limiting our capacity to assess their predictive value. ARG1 was another marker with low signal relative to nonspecific counts in many samples (Supplementary Fig. S9), and therefore its potential favorable predictive value in the CD45 compartment should be cautiously interpreted. These findings could indicate the need for a more rigorous validation of these primary antibodies for future DSP panels. Alternatively, a CD3-restricted compartment could have resulted in an increased signal for some of these markers (23).

In conclusion, this study illustrates the potential of high-plex DSP as a research tool to discover biomarkers of response to immunotherapy in NSCLC. We identified a number of relevant candidate immune predictors in spatial context that show promise for future validation in larger independent cohorts.

Disclosure of Potential Conflicts of Interest

J. Zugazagoitia is an employee/paid consultant for Guardant Health, reports receiving speakers bureau honoraria from Roche, Pfizer, Guardant Health, and NanoString, and other remuneration from Roche. K. Fuhrman is an employee/paid consultant for Nektar and is an advisory board member/unpaid consultant for NanoString Technologies Inc. S. Gettinger is an employee/paid consultant for Nektar and is an advisory board member/unpaid consultant for NextCure. R.S. Herbst is an employee/paid consultant for AbbVie Pharmaceuticals, ARMO Biosciences, AstraZeneca, Biodesix, Bolt Biotherapeutics, Bristol-Myers Squibb, Eli Lilly and Company, EMD Serrano, Genentech/Roche, Genmab, Halozyme, Heat Biologics, IMAB Biopharma, Immunocore, Infinity Pharmaceuticals, Loxo Oncology, Merck and Company, Midas Health Analytics, Mirati Therapeutics, Nektar, Neon Therapeutics, NextCure, Novartis, Pfizer, Sanofi, Seattle Genetics, Shire PLC, Spectrum Pharmaceuticals, Symphogen, Takeda, Tesaro, and Tocagen, reports receiving other commercial research support from AstraZeneca, Eli Lilly and Company, Genentech/Roche, and Merck and Company, and other remuneration from Junshi Pharmaceuticals. K.A. Schalper is an employee/paid consultant for AstraZeneca, Clinica Alemana Santiago, Dynamo Therapeutics, EMD Serono, Merck, Moderna, Pierre Fabre, Shattuck Labs, Takeda, Torque Therapeutics, Ono Pharamaceuticals, Agenus, AbbVie, and Celgene, reports receiving commercial research grants from AstraZeneca, Bristol-Myers Squibb, Eli Lilly, Merck, Moderna, Navigate Biopharma, Pierre Fabre, Surface Oncology, Takeda, and Tesaro, and speakers bureau honoraria from Bristol-Myers Squibb, Merck, Fluidigm, and PeerView. D.L. Rimm is an employee/paid consultant for Biocept, NextCure, Odonate, and Sanofi, reports receiving commercial research grants from AstraZeneca, Cepheid, Navigate BioPharma, NextCure, Lilly, and Ultivue, instrument support from Ventana, Akoya/Perkin Elmer, and NanoString, holds ownership interest (including patents) in PixelGear, is an advisory board member/unpaid consultant for Amgen, AstraZeneca, Cell Signaling Technology, Cepheid, Daiichi Sankyo, GlaxoSmithKline, Konica/Minolta, Merck, NanoString, Perkin Elmer, PAIGE.AI, Roche, Ventana, and Ultivue, and other remuneration from Bristol-Myers Squibb and Rarecyte. No potential conflicts of interest were disclosed by the other authors.

Authors' Contributions

Conception and design: J. Zugazagoitia, S. Gupta, R.S. Herbst, D.L. Rimm
Development of methodology: J. Zugazagoitia, S. Gupta, K. Fuhrman, R.S. Herbst
Acquisition of data (provided animals, acquired and managed patients, provided facilities, etc.): J. Zugazagoitia, S. Gupta, Y. Liu, K. Fuhrman, S. Gettinger, R.S. Herbst
Analysis and interpretation of data (e.g., statistical analysis, biostatistics, computational analysis): J. Zugazagoitia, S. Gupta, Y. Liu, K. Fuhrman, S. Gettinger, R.S. Herbst, K.A. Schalper, D.L. Rimm
Writing, review, and/or revision of the manuscript: J. Zugazagoitia, S. Gupta, Y. Liu, S. Gettinger, R.S. Herbst, K.A. Schalper, D.L. Rimm
Administrative, technical, or material support (i.e., reporting or organizing data, constructing databases): J. Zugazagoitia, D.L. Rimm
Study supervision: J. Zugazagoitia, D.L. Rimm

Acknowledgments

This work was supported by funds from the Yale SPORE in lung cancer P50 CA196530 to S. Gettinger, R.S. Herbst, K.A. Schalper, and D.L. Rimm. J. Zugazagoitia was supported by a Rio Hortega contract from the Carlos III Research Institute (CM15/00196) and a fellowship from the Spanish Society of Medical Oncology. D.L. Rimm received instrument (GeoMx) support from NanoString Inc. The authors thank Lori A. Charette and the staff of Yale Pathology tissue services for expert histology services.

The costs of publication of this article were defrayed in part by the payment of page charges. This article must therefore be hereby marked *advertisement* in accordance with 18 U.S.C. Section 1734 solely to indicate this fact.

Received January 14, 2020; revised March 5, 2020; accepted April 2, 2020; published first April 6, 2020.

References

1. Doroshow DB, Sanmamed MF, Hastings K, Politi K, Rimm DL, Chen L, et al. Immunotherapy in non-small cell lung cancer: facts and hopes. Clin Cancer Res 2019;25:4592–602.
2. Stack EC, Wang C, Roman KA, Hoyt CC. Multiplexed immunohistochemistry, imaging, and quantitation: a review, with an assessment of Tyramide signal amplification, multispectral imaging and multiplex analysis. Methods 2014;70:46–58.
3. Lu S, Stein JE, Rimm DL, Wang DW, Bell JM, Johnson DB, et al. Comparison of biomarker modalities for predicting response to PD-1/PD-L1 checkpoint blockade: a systematic review and meta-analysis. JAMA Oncol 2019 Jul 18 [Epub ahead of print].
4. Merritt CR, Ong GT, Church SE, Barker K, Danaher P, Geiss G, et al. Multiplex digital spacial profiling of proteins and RNA in fixed tissue. Nat Biotechnol 2020;38:586–99.
5. Huang W, Hennrick K, Drew S. A colorful future of quantitative pathology: validation of Vectra technology using chromogenic multiplexed immunohistochemistry and prostate tissue microarrays. Hum Pathol 2013;44:29–38.
6. Spitzer MH, Carmi Y, Reticker-Flynn NE, Kwek SS, Madhireddy D, Martins MM, et al. Systemic immunity is required for effective cancer immunotherapy. Cell 2017;168:487–502.
7. Böttcher JP, Bonavita E, Chakravarty P, Blees H, Cabeza-Cabrerizo M, Sammicheli S, et al. NK cells stimulate recruitment of cDC1 into the tumor microenvironment promoting cancer immune control. Cell 2018;172:1022–37.
8. Hsu J, Hodgins JJ, Marathe M, Nicolai CJ, Bourgeois-Daigneault M-C, Trevino TN, et al. Contribution of NK cells to immunotherapy mediated by PD-1/PD-L1 blockade. J Clin Invest 2018;128:4654–68.
9. Barry KC, Hsu J, Broz ML, Cueto FJ, Binnewies M, Combes AJ, et al. A natural killer-dendritic cell axis defines checkpoint therapy-responsive tumor microenvironments. Nat Med 2018;24:1178–91.
10. Zemek RM, De Jong E, Chin WL, Schuster IS, Fear VS, Casey TH, et al. Sensitization to immune checkpoint blockade through activation of a STAT1/NK axis in the tumor microenvironment. Sci Transl Med 2019;11:eaav7816.
11. Krieg C, Nowicka M, Guglietta S, Schindler S, Hartmann FJ, Weber LM, et al. High-dimensional single-cell analysis predicts response to anti-PD-1 immunotherapy. Nat Med 2018;24:144–53.
12. Binnewies M, Mujal AM, Pollack JL, Combes AJ, Hardison EA, Barry KC, et al. Unleashing type-2 dendritic cells to drive protective antitumor CD4+ T cell immunity. Cell 2019;177:556–71.
13. Zuazo M, Arasanz H, Fernandez-Hinojal G, García Granda MJ, Gato M, Bocanegra A, et al. Functional systemic CD4 immunity is required for clinical responses to PD-L1/PD-1 blockade therapy. EMBO Mol Med 2019;11:e10293.
14. Amaria RN, Reddy SM, Tawbi HA, Davies MA, Ross MI, Glitza IC, et al. Neoadjuvant immune checkpoint blockade in high-risk resectable melanoma. Nat Med 2018;24:1649–54.

15. Koyama S, Akbay EA, Li YY, Herter-Sprie GS, Buczkowski KA, Richards WG, et al. Adaptive resistance to therapeutic PD-1 blockade is associated with upregulation of alternative immune checkpoints. Nat Commun 2016;7:10501.
16. Gao J, Ward JF, Pettaway CA, Shi LZ, Subudhi SK, Vence LM, et al. VISTA is an inhibitory immune checkpoint that is increased after ipilimumab therapy in patients with prostate cancer. Nat Med 2017;23:551–5.
17. Suzuki K, Kadota K, Sima CS, Nitadori J-I, Rusch VW, Travis WD, et al. Clinical impact of immune microenvironment in stage I lung adenocarcinoma: tumor interleukin-12 receptor β2 (IL-12Rβ2), IL-7R, and stromal FoxP3/CD3 ratio are independent predictors of recurrence. J Clin Oncol 2013;31:490–8.
18. Liu Y, Zugazagoitia J, Ahmed FS, Henick BS, Gettinger S, Herbst RS, et al. Immune cell PD-L1 co-localizes with macrophages and is associated with outcome in PD-1 pathway blockade therapy. Clin Cancer Res 2020;26:970–7.
19. Toki MI, Merritt CR, Wong PF, Smithy JW, Kluger HM, Syrigos KN, et al. High-plex predictive marker discovery for melanoma immunotherapy treated patients using digital spatial profiling. Clin Cancer Res 2019;25:5503–12.
20. Herbst RS, Soria J-C, Kowanetz M, Fine GD, Hamid O, Gordon MS, et al. Predictive correlates of response to the anti-PD-L1 antibody MPDL3280A in cancer patients. Nature 2014;515:563–7.
21. Lin H, Wei S, Hurt EM, Green MD, Zhao L, Vatan L, et al. Host expression of PD-L1 determines efficacy of PD-L1 pathway blockade-mediated tumor regression. J Clin Invest 2018;128:805–15.
22. Tang H, Liang Y, Anders RA, Taube JM, Qiu X, Mulgaonkar A, et al. PD-L1 on host cells is essential for PD-L1 blockade-mediated tumor regression. J Clin Invest 2018;128:580–8.
23. Datar I, Sanmamed MF, Wang J, Henick BS, Choi J, Badri T, et al. Expression analysis and significance of PD-1, LAG-3, and TIM-3 in human non-small cell lung cancer using spatially resolved and multiparametric single-cell analysis. Clin Cancer Res 2019;25:4663–73.